

Pattern formation of Rho GTPases in single cell wound healing

Cory M. Simon^a, Emily M. Vaughan^{b,c}, William M. Bement^{b,c,d}, and Leah Edelstein-Keshet^a

^aDepartment of Mathematics, University of British Columbia, Vancouver, BC V6T 1Z2, Canada; ^bProgram in Cellular and Molecular Biology, ^cDepartment of Zoology, and ^dLaboratory of Cellular and Molecular Biology, University of Wisconsin–Madison, Madison, WI 53706

ABSTRACT The Rho GTPases—Rho, Rac, and Cdc42—control an enormous variety of processes, many of which reflect activation of these GTPases in spatially confined and mutually exclusive zones. By using mathematical models and experimental results to establish model parameters, we analyze the formation and segregation of Rho and Cdc42 zones during *Xenopus* oocyte wound repair and the role played by Abr, a dual guanine nucleotide exchange factor–GTPase-activating protein, in this process. The Rho and Cdc42 zones are found to be best represented as manifestations of spatially modulated bistability, and local positive feedback between Abr and Rho can account for the maintenance and dynamic properties of the Rho zone. In contrast, the invocation of an Abr-independent positive feedback loop is required to account for Cdc42 spatial bistability. In addition, the model replicates the results of previous *in vivo* experiments in which Abr activity is manipulated. Further, simulating the model with two closely spaced wounds made nonintuitive predictions about the Rho and Cdc42 patterns; these predictions were confirmed by experiment. We conclude that the model is a useful tool for analysis of Rho GTPase signaling and that the Rho GTPases can be fruitfully considered as components of intracellular pattern formation systems.

Monitoring Editor

Alex Mogilner
University of California, Davis

Received: Aug 29, 2012

Revised: Nov 13, 2012

Accepted: Dec 5, 2012

INTRODUCTION

The ability to rapidly assemble transient cytoskeletal arrays based on actin filaments (F-actin) at the plasma membrane underlies an enormous number of fundamental cellular processes, including cytokinesis, cell repair, and cell locomotion. Thus, understanding the means by which such arrays are controlled is of considerable interest. Although there is significant variation in the details of both the composition and the regulation of transient cytoskeletal arrays, which include such diverse structures as the cytokinetic apparatus and the

actomyosin networks associated with exocytotic and endocytotic processes (Bement *et al.*, 2006), it is clear that the Rho class GTPases Rho, Rac, and Cdc42 play critical roles in formation of most, if not all such structures. The active (GTP-bound) Rho GTPases direct formation of transient cytoskeletal arrays via association with the plasma membrane and stimulation of effector proteins that, when active, exert a variety of effects on the F-actin cytoskeleton (Jaffe and Hall, 2005). For example, Rho is best known for activating effector proteins such as Rho kinase, which promotes myosin-2 activation, and formins, which promote assembly of unbranched actin filaments. Cdc42 and Rac are best known for activating effector proteins such as N-WASP and the p21-activated kinases, which can then regulate Arp2/3-dependent actin assembly of branched actin networks.

Rho GTPases are subject to regulation via proteins that modulate their nucleotide-binding state. GTPase activating proteins (GAPs) promote hydrolysis of GTP to GDP by the GTPases and thus result in their inactivation. Guanine nucleotide dissociation inhibitors (GDIs) bind to the inactive GTPases and maintain them in the inactive form in the cytoplasm. Guanine nucleotide exchange factors (GEFs) promote the exchange of GDP for GTP by the GTPases, thus activating them and completing the cycle (Jaffe and Hall, 2005).

This article was published online ahead of print in MBcC in Press (<http://www.molbiolcell.org/cgi/doi/10.1091/mbc.E12-08-0634>) on December 21, 2012.

Address correspondence to: Cory M. Simon (corymsimon@gmail.com), Leah Edelstein-Keshet (keshet@math.ubc.ca).

Abbreviations used: GAP, GTPase-activating protein; GDI, guanine nucleotide dissociation inhibitor; GEF, guanine nucleotide exchange factor; SS, steady state.

© 2013 Simon *et al.* This article is distributed by The American Society for Cell Biology under license from the author(s). Two months after publication it is available to the public under an Attribution–Noncommercial–Share Alike 3.0 Unported Creative Commons License (<http://creativecommons.org/licenses/by-nc-sa/3.0>). “ASCB®,” “The American Society for Cell Biology®,” and “Molecular Biology of the Cell®” are registered trademarks of The American Society of Cell Biology.

Transient cytoskeletal arrays assemble in discrete locations, and visualization of active Rho GTPases indicates that this results from formation of spatially confined activity “zones” at the sites of array assembly (Bement *et al.*, 2006). Within a given zone, the activity of the GTPase in question is approximately twofold to fivefold higher than in regions immediately outside the zones. We henceforth use “zone” to describe the region where either Rho or Cdc42 is active beyond basal levels (see also Benink and Bement, 2005; Bement *et al.*, 2006). A growing body of evidence suggests that the confinement of the zone reflects rapidly local flux of the GTPases through the GTP cycle (Bement *et al.*, 2005, 2006; Miller and Bement, 2009; Yoshida *et al.*, 2009; Burkel *et al.*, 2012). The tight localization of the active GTPases within zones likely permits focal regulation of GTPase targets, as revealed by comparison of such targets to zones (e.g., Bravo-Cordero *et al.*, 2011).

Because transient cytoskeletal arrays generally require the spatially and temporally coordinated action of both F-actin and myosin-2, most such arrays entail control by more than one Rho GTPase. For example, during single cell wound repair, two concentric zones of Cdc42 and Rho encircle the damaged area (Benink and Bement, 2005). The Cdc42 zone directs formation of a region of highly dynamic actin, whereas the Rho zone directs formation of a region enriched in active myosin-2. Similarly, during polar body emission—a highly asymmetric form of cytokinesis—a ring-like Rho zone encloses a patch-like zone of Cdc42 activity (Ma *et al.*, 2006), and, again, each zone directs formation of a functionally distinct cytoskeletal array (Zhang *et al.*, 2008). Similarly, during cell locomotion, small, discontinuous zones of Rho and Cdc42 exist, with active Rho occupying regions from which active Cdc42 and/or Rac are excluded, and vice versa (Machacek *et al.*, 2009). Such segregation is presumed to result from “cross-talk,” in which the activity of one GTPase suppresses or enhances the activity of other GTPases either directly or indirectly (Pertz, 2010). Such positive/negative feedbacks have been shown to lead to complex temporal dynamics (bistability or cycles), as well as to spatial gradients and patterns in cells (Kholodenko, 2006).

Surprisingly, the high degree of spatial precision exhibited by GTPase zones does not necessarily reflect obviously precise upstream signaling events. For example, during single cell wound repair, an initially crude signal—local elevation of calcium around the wound (Clark *et al.*, 2009)—is somehow rapidly converted into the concentric Rho and Cdc42 zones (Benink and Bement, 2005).

To better understand how some of the features of Rho GTPase zones arise, we chose for analysis the *Xenopus* oocyte wound repair model, based on its relative simplicity (see prior discussion) and the recent observation that the behavior of the GTPase zones during wound repair is controlled by Abr, a dual GEF-GAP (Vaughan *et al.*, 2011). In vitro, Abr is a GEF for both Rho and Cdc42 and a GAP for Cdc42 but not Rho (Chuang *et al.*, 1995). During wound repair, Abr behaves in a manner consistent with it serving as a GEF for Rho and a GAP for Cdc42, and it has been proposed to mediate local cross-talk between Rho and Cdc42 during wound healing (Vaughan *et al.*, 2011). By using a combination of mathematical models and experimental results to establish model parameters, we find that several important features of Rho GTPase pattern formation during oocyte wound repair can be explained based on the known activities of Abr. We also find that a minimal model not only captures the results of previous experimental manipulations, but it also accurately predicts nonintuitive outcomes of new experiments in which wounds are made at different distances from each other. Finally, the results support the general notion that the Rho GTPases and their regulators can be considered parts of an intracellular pattern formation

system, analogous to the systems that govern developmental pattern formation.

RESULTS

Evidence for spatial bistability during GTPase pattern formation

Our first goal was to assess the basic features of GTPase activation during the oocyte wound response to characterize potential constraints on zone behavior. The behavior of active Rho and Cdc42 was assessed by four-dimensional (4D) time-lapse imaging using green fluorescent protein (GFP)-rGBD (a probe for active Rho) and monomeric red fluorescent protein (mRFP)-wGBD (a probe for active Cdc42) as previously described (Benink and Bement, 2005). Fluorescence intensities in different regions of the cell were measured from 4D image series. Before wounding, the activity of Rho and Cdc42 is uniformly low over the surface of the cell (Figure 1A) and remains that way indefinitely unless subject to damage. However, upon wounding, Rho and Cdc42 activity rises to maximal levels within ~60–80 s and then reaches a plateau, which is maintained for ~2–3 min, after which time the zones move z-ward (i.e., toward the cell interior) and can no longer be followed (Figure 1A). Over the same time period, regions outside the zones maintain background levels of Rho and Cdc42 activity (Figure 1, B and C). With known rates of GTPase diffusion and inactivation/GDI sequestering (Postma *et al.*, 2004), these regions of high activity would be expected to decay over this time scale without a mechanism for sustaining them. These behaviors are reminiscent of “spatial bistability.” Bistability denotes the existence of both low- and high-activity states in a time-dependent system, with some threshold separating the two states. *Spatial* bistability refers to spatially distributed systems in which the activity or abundance of a given pattern regulator is high within a limited spatial zone and at background levels elsewhere (e.g., Wang and Ferguson, 2005), with some transition layer connecting these regions (Goehring *et al.*, 2011). Such regions often develop progressively, with an initially shallow gradient becoming sharper over time, as observed here in the RhoA and Cdc42 activity in Figure 1, B and C. Often spatial bistability results when bistable reaction kinetics are coupled with spatial diffusion of the reactants. The presence of a threshold in bistability implies that a perturbation must be large enough to switch the system from one state to another (Goehring *et al.*, 2011). This characteristic is necessary to avoid the formation of spontaneous regions of activity from small, random fluctuations in an unwounded cell. A common theme in chemical systems that engender bistability is a positive feedback loop (Ferrell and Xiong, 2001), such as the one between RhoA and Abr, but other mechanisms for bistability are possible (Craciun *et al.*, 2006).

Cross-talk during GTPase pattern formation

We next compared spatial patterns of active Rho and Cdc42 to each other. To accomplish this, we generated kymographs from 10-pixel-wide slices through one side of the wound (Figure 2A) and converted them into double-label line-scan intensity plots (Figure 2B and Supplemental Movie S1). The kymograph and plots make evident what is difficult to see in the time-lapse series shown in Figure 1: Although active Rho and Cdc42 ultimately segregate into discrete zones, initially their activity is more broadly distributed and in fact shows significant overlap (Figure 2B). However, between ~30 and 70 s, coincident with the sharp rise of Rho and Cdc42 activity (see Figure 1B), as Rho activity rises and resolves into a sharper peak, the peak of local Cdc42 activity that initially overlapped with it is lost in that region and accumulates behind it (relative to the wound; Figure 2B). Thus the GTPase

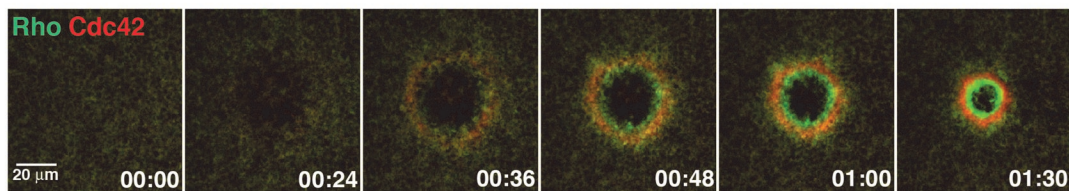
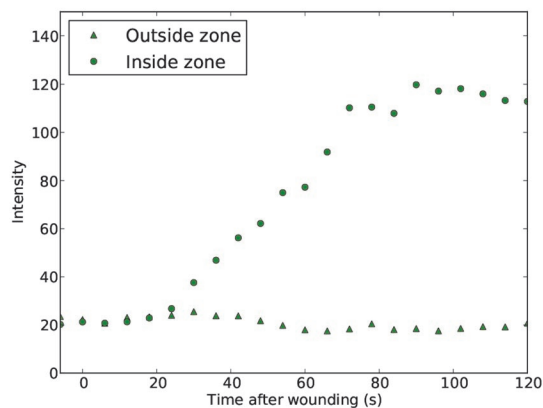
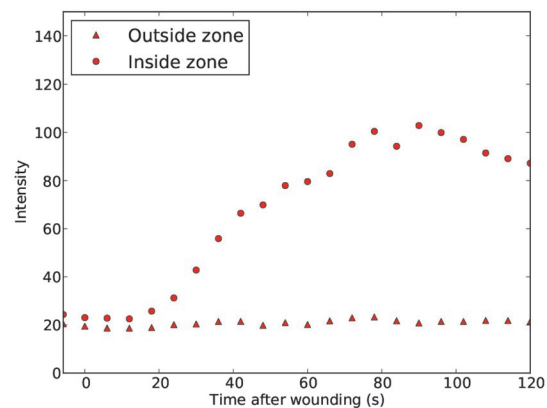
A**B****Rho Activity****C****Cdc42 Activity**

FIGURE 1: Basic features of GTPase response to wounding. (A) Time course showing individual frames generated from a 4D movie of active Rho (green) and active Cdc42 (red) during oocyte wound response. Each frame represents a projection of six optical sections. Time after wounding in minutes:seconds. (B) Plot of fluorescence intensity of GFP-rGBD (RhoA activity) within the zone at different times after wounding and intensity at regions 10 μm outside the zone. Each point represents an average of eight measurements taken at different positions within or outside the zone. The positions of the zone (and thus the measurements) were determined from line intensity scans and thus represent moving frames of reference. (C) Plot of fluorescence intensity of RFP-wGBD (Cdc42 activity) within the zone at different times after wounding and intensity at regions 10 μm outside the zone. Each point represents an average of eight measurements taken at different positions within or outside the zone as in B.

zones are not initially separate but arise from regions of overlapping and relatively low Rho and Cdc42 activity. This progressive amplification and segregation resembles processes observed in developmental pattern formation, which are often underlain by both positive and negative feedback between signaling molecules (see *Discussion*).

Basic models

The foregoing results provided an empirical framework with which to test different models designed to account for zone behavior. We developed a reaction-diffusion-advection model to analyze the processes of zone maintenance and segregation and the ability of the dual GEF-GAP Abr to account for the observed behaviors of the zones. Treatment of Rho GTPases using reaction-diffusion-advection equations naturally follows from their known diffusion properties and interactions.

The models are based on the following assumptions: 1) Local barriers to diffusion are not needed. Thus the system is treated strictly in terms of activation, inactivation, cross-talk, and feedback between GTPases and GEF/GAPs/GDIs. This assumption is based on the observation that there are no apparent physical structures between the zones, as well as on the fact that zones

form and segregate after the disruption of either F-actin or microtubules (Benink and Bement, 2005). 2) Abr has GEF activity toward Rho and Cdc42 and GAP activity toward Cdc42 but not Rho. This assumption is based on direct *in vitro* measurements of the GEF and GAP activity and specificity of Abr (Chuang *et al.*, 1995). 3) Abr is targeted to wounds via interaction with active Rho. This assumption is based on the demonstration that Abr targeting to wounds requires active Rho and that exogenously activated Rho recruits Abr to the plasma membrane in unwounded cells (Vaughan *et al.*, 2011). 4) Wounded plasma membrane is not capable of supporting Rho GTPase activity and thus defines the maximum inner limit of the GTPase zones. This assumption is based on the observation that the centers of wounds do not have active Rho or Cdc42 (Benink and Bement, 2005) or phosphatidylserine (unpublished results), a normal lipid component of the plasma membrane.

Three interrelated models were developed and sequentially tested (Figure 3). In Model 1, just the Abr-Rho module is considered, in which Abr serves as a GEF for, and undergoes positive feedback with, Rho. In Model 2, the Abr-Rho module and Cdc42 are considered, in which the Abr serves as both a GAP and a GEF for Cdc42. In Model 3, the Abr-Rho module and Cdc42 models

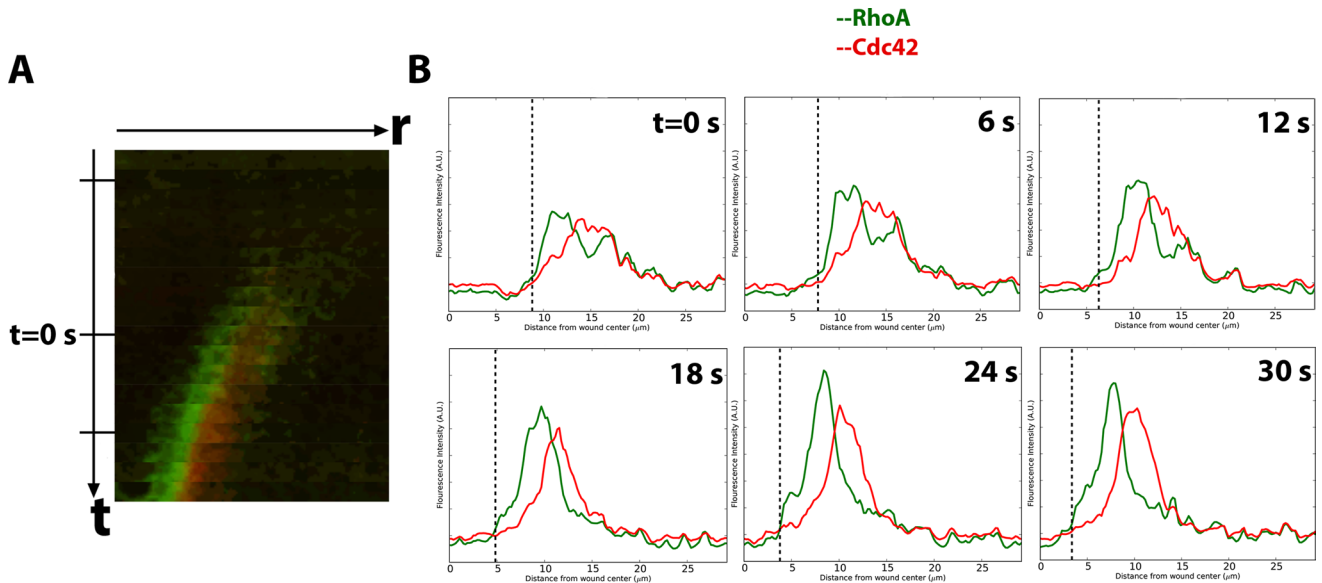


FIGURE 2: Segregation of the Rho and Cdc42 zones. (A) Data kymograph of 10-pixel-wide slices from a movie used to generate Figure 1A, showing active Rho (green) and active Cdc42 (red). Here t is time in seconds, r is distance from the wound center (spans $40\ \mu\text{m}$), and the wound is toward the left of the kymograph. The first, second, and third tick marks indicate the time of wounding, the initial condition (time zero) for the model, and the final simulation time, respectively. (B) Plots of intensity profiles (data) of probe for active Rho (green) or active Cdc42 (red) corresponding to slices presented in A. Dashed line represents the wound edge.

are considered together with the addition of a positive feedback loop for Cdc42. For all models, Rho and Cdc42 are considered to be in flux on and off the membrane, with the active form associated with the membrane and the inactive form in the cytoplasm (Figure 3A), and all models incorporate myosin-2-powered advection. Note that we do not explicitly track or model myosin or actin. Instead we assume a flow of cortex (and membrane-associated GTPases) toward the wound center. The radial profile of the flow velocity is constrained by the continuity equa-

tion, and we fit the magnitude to wound location data. For each reaction shown in Figure 3, we assume a simple mathematical description and only modify that if necessary. The models focus on the period of time during which the overlapping, shallow Rho and Cdc42 activity gradients are converted into steep, mutually exclusive zones. This corresponds to the ~ 48 - to ~ 78 -s interval after wounding in the typical cell (see Figure 2); for the sake of convenience 48 s after wounding is considered time zero for the model.

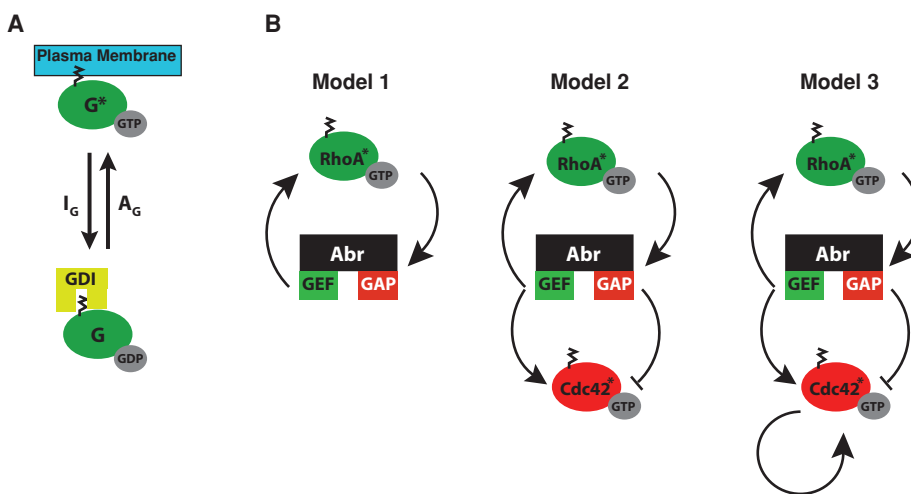


FIGURE 3: Models of GTPase pattern formation. (A) Schematic showing the basic scheme of Rho or Cdc42 association with the plasma membrane. (B) Schematic showing the three basic models generated and tested in this study. Model 2 contains proposed interactions based on experiments, and Model 3 contains a positive feedback loop for Cdc42 postulated by our model.

Spatial bistability of the RhoA–Abr module requires nonlinear kinetics

We first tested Model 1 to assess the hypothesis that the bistability can arise from RhoA–Abr interactions independent of the Cdc42 module, as indicated by empirical results (Vaughan *et al.*, 2011; see the Supplemental Material, Section S2.1). The activation rate of Rho ($A_{\text{free rho}}$) includes a constant term to represent Rho GEFs other than Abr and a term that is an increasing function of Abr to represent the GEF activity of Abr. The binding of Abr to active Rho is modeled with mass action kinetics. When $A_{\text{free rho}}$ depends linearly on localized Abr, bistability is not achieved and Rho has only one steady state (Figure 4A). Similarly, when the relationship between $A_{\text{free rho}}$ and localized Abr are represented by Michaelis–Menten kinetics, bistability cannot be achieved (Figure 4B). In contrast, if a Hill function (i.e., sigmoidal kinetics) is used for the relationship between $A_{\text{free rho}}$ and localized Abr, spatial

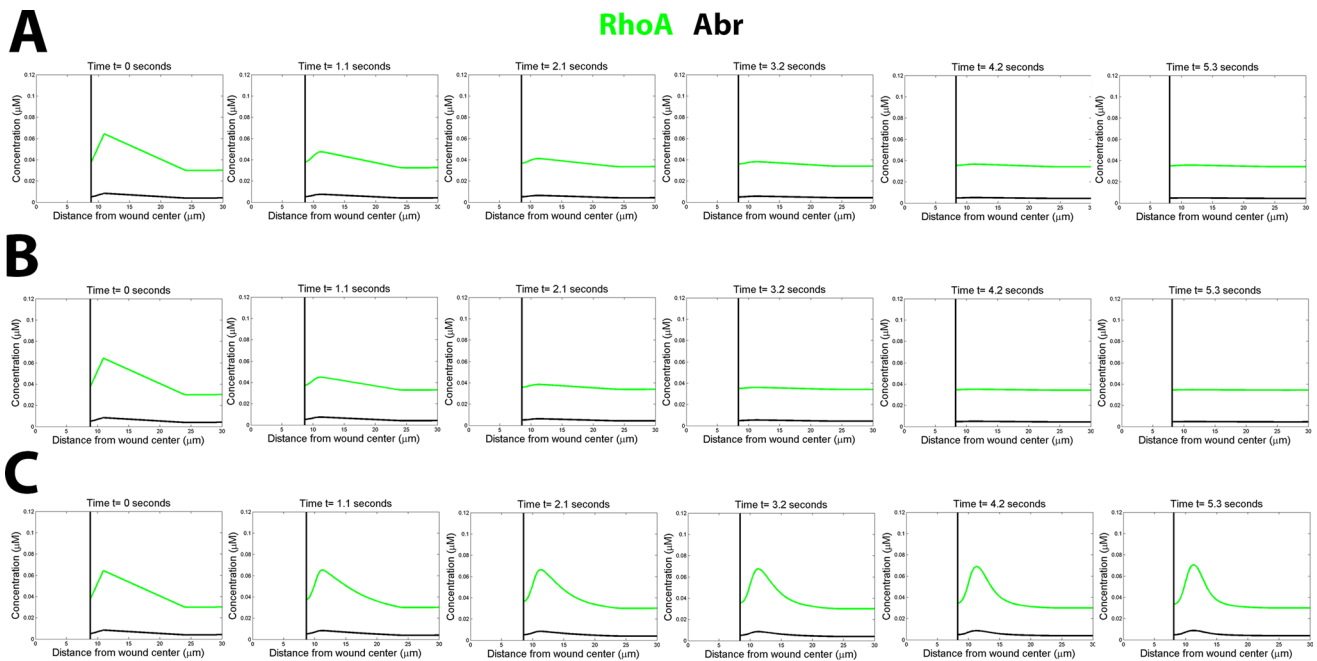


FIGURE 4: Model 1 simulations of RhoA activity and Abr vs. distance from the center of the wound. (A) Linear kinetics for the Abr-mediated activation of Rho result in any stimulus of RhoA or Abr decaying to the background level for all parameter regimes. (B) Michaelis–Menten kinetics fail to sustain the pattern as well. (C) A Hill function for the Abr-mediated Rho activation results in the sustenance of the Rho pattern, as observed in vivo.

bistability is achieved, with two stable steady states being observed for a certain parameter range (Figure 4C). On the basis of this nonlinear form of $A_{\text{free rho}}$, the reaction terms $f_{\text{abr-rho}}$ and $f_{\text{free rho}}$ result in a situation in which the rates of activation (A) and inactivation (I) can be stably balanced in two different states, yielding for Rho and Abr both a low and a high steady state far and near the wound, respectively. In other words, if the kinetics between the interactions of Rho and Abr are sufficiently nonlinear, the system is endowed with bistability, which explains how high levels of Rho activity can be maintained in a narrow region. (Compare Figure 4 to Figure 1B.)

Spatial bistability of Cdc42 requires positive feedback and nonlinear kinetics

We next sought to incorporate Cdc42 into the results by testing Model 2 (see Figure 3 and the Supplemental Material, Section S2.2), building upon the successful model for the Rho–Abr module that invoked sigmoidal activation kinetics. To account for the other (non Abr) GEFs and GAPs that we do not explicitly model, we included a constant term in both A_{cdc} and I_{cdc} . We model the GEF and GAP activity of the localized Abr with simple, mass action kinetics (linear terms with respect to Abr-bound RhoA) in A_{cdc} and I_{cdc} . Under these assumptions (Model 2), the model fails to account for the observed Cdc42 peak and instead results in any Cdc42 activity decaying to its basal level (Figure 5A). Mathematically, this is due to a lack of bistability. Both linear and nonlinear kinetics for Abr regulation of Cdc42 were insufficient to capture spatial bistability (see the Supplemental Material, Section S2.2). Because Cdc42 maintains two disparate activity levels outside of the RhoA zone, where Abr is at a uniform level, any nonlinearity in the Abr regulation of Cdc42 or interaction with free active RhoA cannot possibly account for two disparate steady states outside of the RhoA zone.

Accordingly, we developed Model 3, which invokes Cdc42-dependent, Abr/Rho-independent positive feedback (Figure 3). Three versions of Model 3 were tested: one in which the Cdc42

autocatalysis was assumed to have linear kinetics, one in which it was assumed to have Michaelis–Menten kinetics, and one in which it was assumed to have Hill kinetics. As observed with Rho, linear kinetics (Figure 5B) or Michaelis–Menten kinetics (unpublished data) failed to reproduce Cdc42 bistability, whereas Hill kinetics successfully captured the required bistability (Figure 5C; Supplemental Movie 1). Further, comparison of the patterns of changes observed in the Rho and Cdc42 profiles over time in the model paralleled those observed in vivo. Specifically, the initial overlap of broad Rho and Cdc42 gradients is rapidly converted into mutually exclusive, concentric zones, with the Cdc42 zone outside (i.e., distal to the wound) and the Rho zone inside (i.e., proximal to the wound). As expected, based on the results presented, the segregation occurs spontaneously from the initial conditions when all of the features of Model 3 are present but fails in simpler models when one or more of the proposed interactions are lacking (Figures 4, A and B, and 5, A and B).

Comparison of the in silico model to Abr manipulations in vivo

To further assess the experimental fidelity of Model 3, we systematically compared results of previous in vivo experiments to model simulations of those experiments.

In the first experiment, with overexpression of wild type Abr, the Rho zone broadens to approximately twice its normal width while maintaining a normal level of intensity as the concentration of Abr is successively increased (Vaughan *et al.*, 2011). Meanwhile, the Cdc42 zone decreases in intensity and is overtaken by the Rho zone (Vaughan *et al.*, 2011). We mimicked this manipulation in silico by increasing the value of the cytosolic Abr concentration, $[A]$. After this manipulation, Model 3 captures both the loss of the Cdc42 zone and the spreading of the Rho zone without a significant increase in intensity (Figure 6A and Supplemental Material, Section S6.1).

The model, however, predicts that, at the highest levels of Abr overexpression (22% above normal background cytosolic levels),

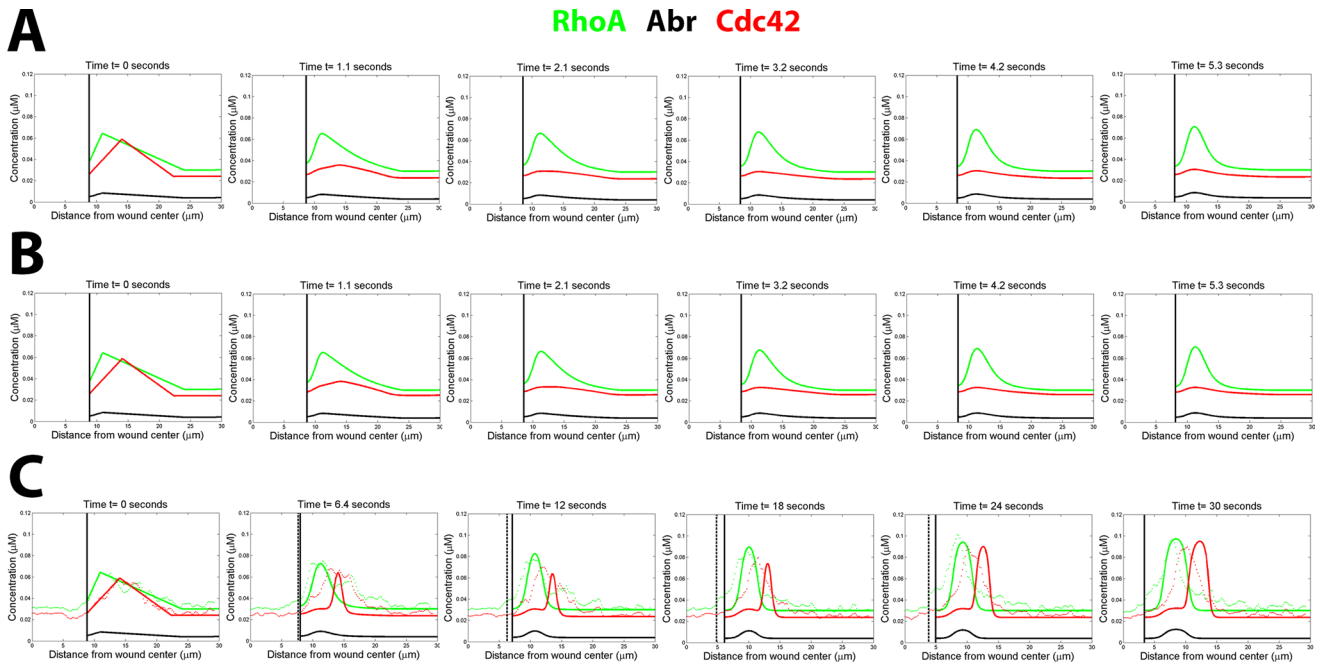


FIGURE 5: Model 2 and 3 simulations of Cdc42 activity vs. distance from the center of the wound. We use the RhoA–Abr Model 1 described earlier. (A) Simulation of Model 2. For every parameter regime and any stimulus of Cdc42, any Cdc42 activity outside of the RhoA zone will decay to the background level without positive feedback for Cdc42. (B) Model 3 with a linear form of Cdc42 autocatalysis fails to capture the maintenance of the Cdc42 zone. (C) Model 3 with a Hill-function representation of Cdc42 autocatalysis results in the sustenance of the Cdc42 peak, as observed in vivo. The experimental intensity profiles from Figure 2B are plotted as points with the final Model 3 simulation. The simulated (solid) and experimental (dashed) wound edge is indicated with the black, vertical line.

the Rho zone will fill the entire field, as the Rho–Abr system is unable to attenuate the positive feedback in the low steady state and becomes monostable only with the high steady state. Although this is likely due to the mathematical assumptions (constant cytosolic concentrations, mass action binding of Rho to Abr) breaking down, a potential biological explanation for this discrepancy is that the trailing edge of the Rho zone can direct the recruitment of a GAP that limits the spread of the Rho zone, a possibility not modeled in the present study but consistent with findings from previous work (Burkel *et al.*, 2012). It is also formally possible that higher levels of Abr expression than those achieved in the experimental study of Vaughan *et al.* (2011) might produce the predicted global Rho activation.

In the next experiment, involving the expression of a GEF-dead Abr mutant that nonetheless localizes with active Rho, the Cdc42 zone collapses and the Rho zone is greatly attenuated (Vaughan *et al.*, 2011). We mimicked the loss of GEF activity in this manipulation by decreasing the parameters k_1 and k_5 , which govern Abr-mediated activation in $A_{\text{free rho}}$ and A_{cdc} , and we mimicked the effects of overexpression by increasing $[A]$. After this manipulation, both the RhoA and Cdc42 zones fail to form with a sufficient decrease in k_5 and increase in $[A]$ (Figure 6B and Supplemental Material, Section S6.2). The Rho zone collapses because the positive reinforcement mechanism is not present with GEF-dead Abr. The Cdc42 zone collapses because of two factors: an increase in the level of the Cdc42 GAP activity due to overexpression of the mutant (which still has Cdc42 GAP activity) and the loss of Cdc42 GEF activity.

In the next experiment, involving the expression of a GAP-dead Abr mutant that nonetheless localizes with active Rho, both the Rho and Cdc42 zones persist, but they broaden and bleed into each other (Vaughan *et al.*, 2011). We mimicked this manipulation by decreasing k_8 , the model parameter that represents Abr-mediated

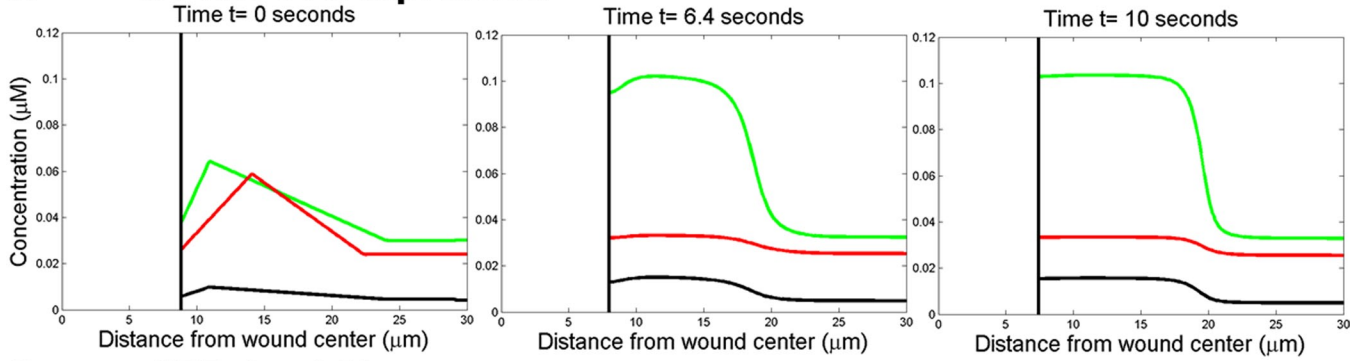
inactivation of Cdc42. As in the GEF-dead mutant manipulations, overexpression was mimicked by increasing $[A]$. For modest changes (75% for k_8 and 20% for $[A]$), the model results in broadening of the Rho and Cdc42 zones and their bleeding into each other, consistent with the in vivo results (Figure 6C and Supplemental Material, Section S6.3). For more extreme changes in parameters, the system cannot attenuate the positive feedback from Abr overexpression and maintains only the high steady state. For Cdc42, this in silico experiment is sensitive to parameter changes because the increased levels of activation due to Abr (which still has its GEF domain) overexpression is exacerbated by the loss of the ability of Abr to inactivate Cdc42.

In the next experiment, involving the microinjection of C3 exoenzyme, which specifically and irreversibly inactivates Rho, Abr is not recruited (Vaughan *et al.*, 2011), the Rho zone fails to form, and the Cdc42 zone broadens and increases in intensity (Benink and Bement, 2005). We mimicked this manipulation by decreasing the Rho activation terms k_1' and k_1 . Consistent with the in vivo results, the Rho zone fails to form, Abr is not recruited, and the Cdc42 zone increases in intensity and broadens (Figure 6D and Supplemental Material, Section S6.4). The results can be understood based on the following model features: Rho inhibition results in less Abr recruitment, simultaneously reducing I_{cdc} and A_{cdc} . Owing to the relative strengths of these activities, the Cdc42 module retains its bistable property, and the steady-state value of Cdc42 within the zone is elevated.

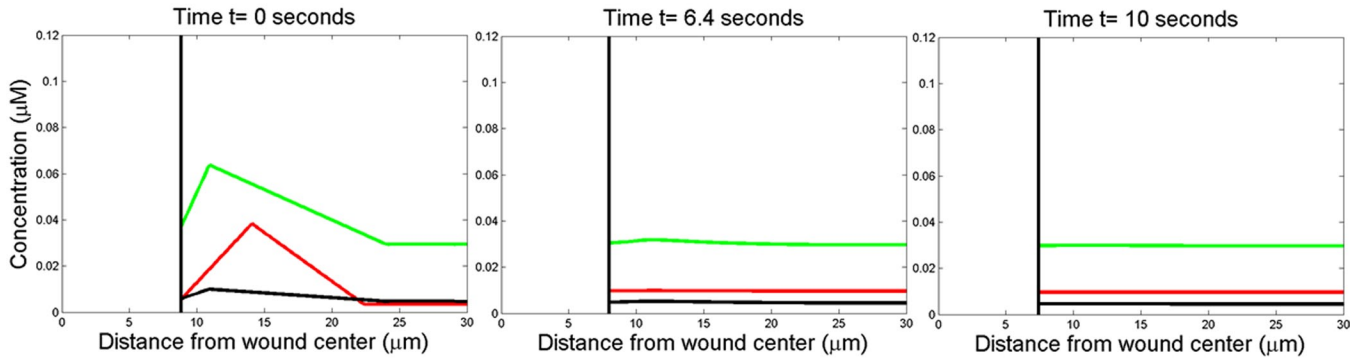
To visualize the model predictions graphically, we plotted phase portraits of the Abr–Rho (two-equation) system and of the (single) Cdc42 dynamics in Figure 7. Curves shown in green-black are, respectively, the Rho and Abr nullclines in the Abr–Rho plane, whose intersections are steady states. These are not to be confused with

RhoA Abr Cdc42

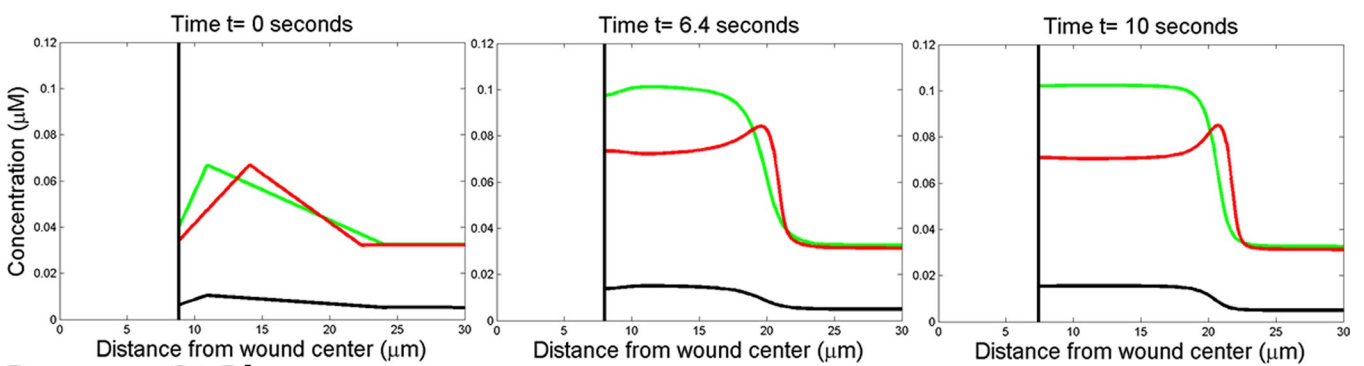
A WT Abr overexpression



B GEF-dead Abr



C GAP-dead Abr



D C3 Rho

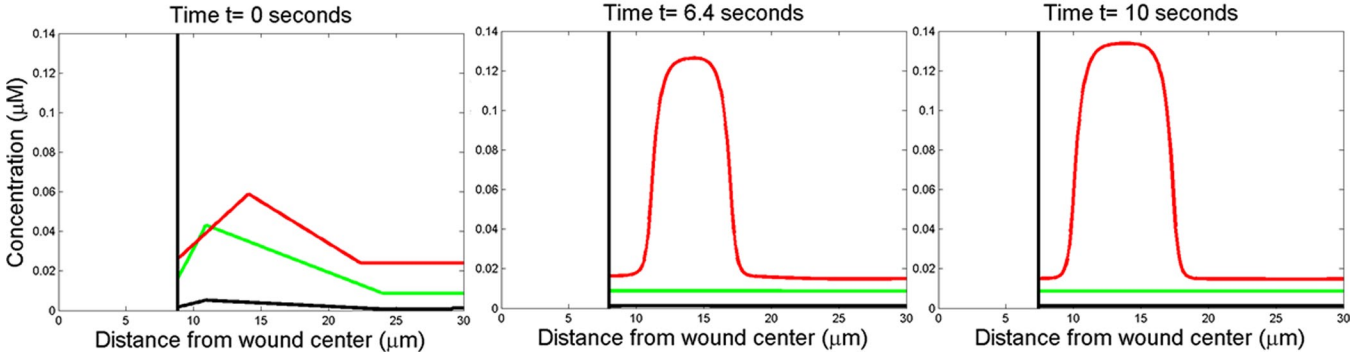


FIGURE 6: In silico experiments to recapitulate in vivo results. (A) To model WT Abr overexpression, [A] is increased by 20%. The RhoA zone broadens to overtake the Cdc42 zone but does not significantly increase in intensity. (B) On overexpression of GEF-dead Abr, the RhoA and Cdc42 zones cannot be sustained. (C) On overexpression of GAP-dead Abr, the zones overlap and broaden in comparison to controls. (D) On C3 inactivation of RhoA, the Cdc42 system retains its bistable property and its pattern still forms. The Cdc42 activity zone brightens due to an elevated high steady state and broadens since the Rho zone is not present to suppress it in the region closer to the wound.

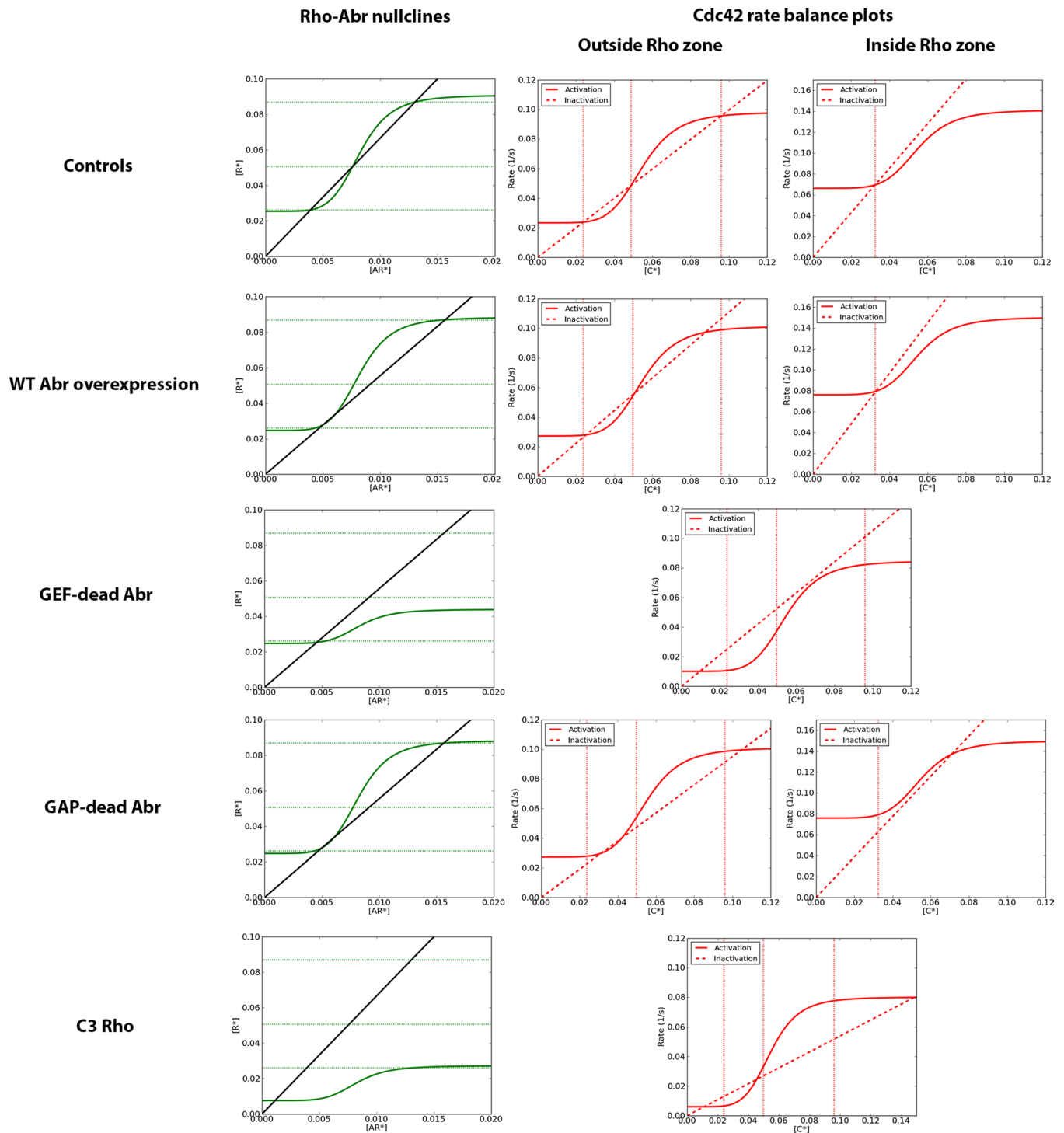


FIGURE 7: Model phase portraits reveal the effect of *in silico* experiments on the number and values of steady states. Left, Abr-Rho phase plane showing active Rho (green) and Abr (black) nullclines. Steady states (SS) are at points of intersection. For comparison, SS Rho activity levels for the controls are indicated with horizontal lines. Red diagrams, dC^*/dt vs. C^* (where C^* = active Cdc42), showing rate of activation (solid) and inactivation (dotted) (SS Cdc42 activity levels for controls are indicated by the vertical lines.) Top, “control” (WT) simulations. Second row, WT Abr overexpression (as in Figure 6A). Third row, GEF-dead Abr (as in Figure 6B). Fourth row, GAP-dead Abr (as in Figure 6C). Last row, C3 Rho (as in Figure 6D). Note the disappearance and/or shifting steady-state values in the distinct treatments. Also note the higher turnover rates inside the Rho zone by comparing the ordinates in columns 1 and 2.

the Cdc42 rate balance plots (red), where both the activation rate (solid red) and the inactivation rate (dotted red) curves depict dC^*/dt versus C^* (where C^* is active Cdc42 level). Steady states are also at intersections of these curves, where activation and inactivation of

Cdc42 are balanced. Cdc42 dynamics depend on Rho and Abr levels, and thus have distinct shapes inside and outside the wound-patterning zone, as shown. From such plots, we can understand how manipulations described in this article affect model properties

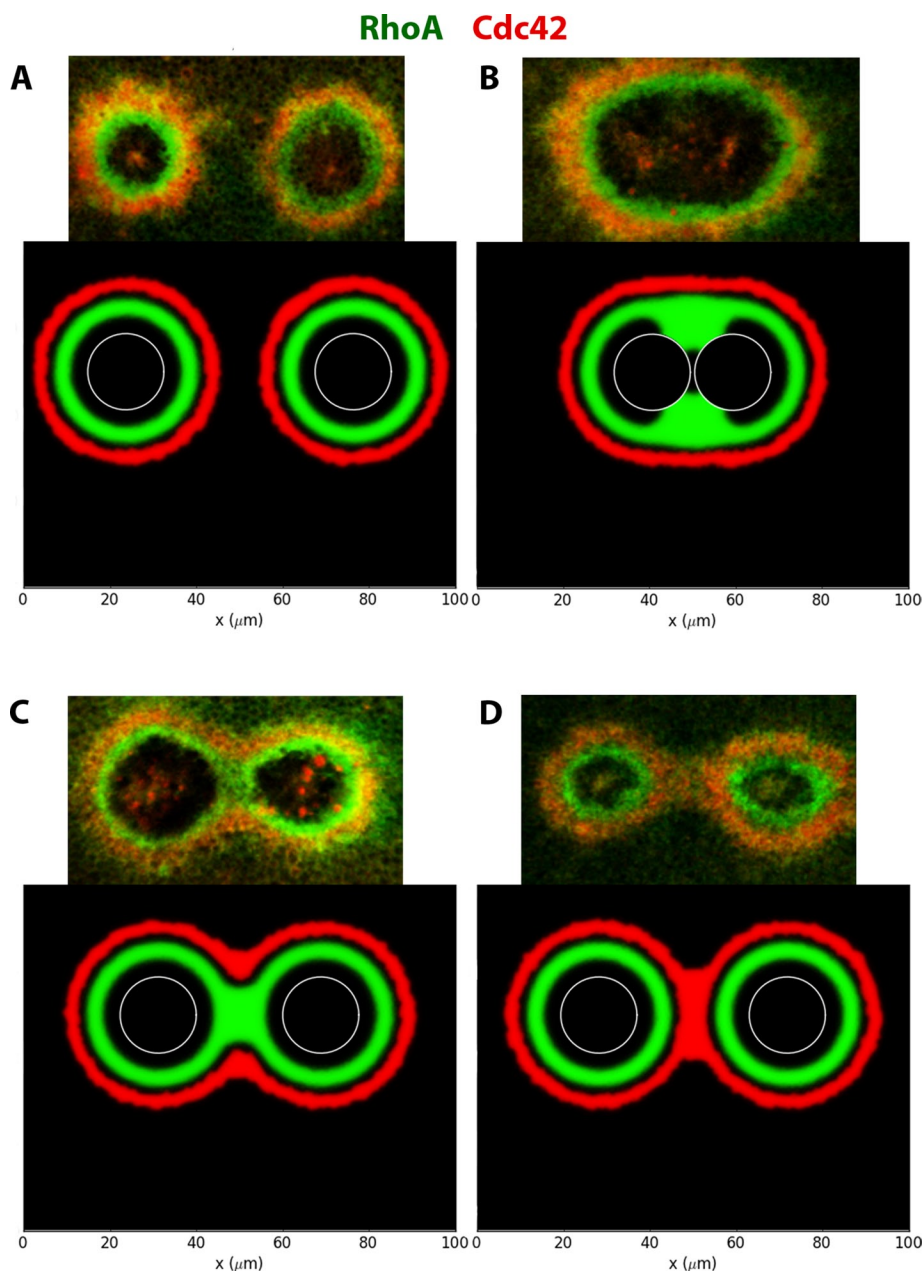


FIGURE 8: Two wound simulations (bottom) and experiments (top). (A) When the wounds are far apart ($35 \mu\text{m}$ in silico), they behave independently. (B) When the wounds are very close ($1 \mu\text{m}$ in silico), they behave as a single wound surrounded by single oval-shaped zones of Rho and Cdc42. (C) When wounds are close enough for the initial Rho gradients to overlap ($20 \mu\text{m}$ in silico), the Rho zones between the wounds fuse together to create a zone wider than twice the width of that in a single control wound. The Rho recruits enough Abr to suppress the Cdc42 in this region with its GAP domain. (D) When wounds are close enough to have overlapping Cdc42 gradients but not significantly overlapping Rho gradients ($26 \mu\text{m}$ in silico), the Cdc42 zones between the wounds fuse together to create a zone more than twice the width of that in a single control wound.

and, in particular, the number of steady states, the presence or absence of bistability, and the values of steady-state GTPase intensity levels. In particular, the difference between the lowest two steady states represents the “threshold” that has to be breached to switch the system to its locally high GTPase-activity state. For a fixed initial gradient from the wound center, a low threshold means that a large region will be induced (by bistability) to jump to a high-activity steady state. (Conversely, a higher threshold decreases the region so induced.) This links steady-state levels and threshold size to

pattern zone width. We first show a control (WT) case: Both Rho–Abr and Cdc42 “outside zone” have three steady states (the middle one is unstable), a hallmark of bistability. Cdc42 has but one lower-activity steady state inside the zone (monostability) due to distinct self- and Abr-induced activation/inactivation rates in the zone environment. The single, low steady state of Cdc42 inside the Rho zone explains why the Cdc zone does not overlap the Rho zone. In WT Abr overexpression, the threshold for Rho drops, broadening the Rho zone. Rho intensity is scarcely affected, due to its saturating activation rate. Cdc42 is bistable outside but monostable inside the Rho zone (a single steady-state activity level). Consequently the Cdc42 zone contracts not because its threshold is lower but because expansion of the Rho zone suppresses Cdc42 in the region where Cdc42 would normally be present. In both GEF-dead Abr and C3 Rho, Rho–Abr is monostable at low levels, whereas Cdc42 is bistable in the latter but not the former case. This explains why the Cdc42 zone survives in the C3 Rho experiment but not in the GEF-dead Abr experiment. Although the threshold for Cdc42 during C3 Rho is not lower than in controls, the zone still broadens because the Rho zone is not there to suppress Cdc42 in the region closer to the wound. For GAP-dead Abr, the Rho zone resembles the WT Abr overexpression case, but the bistable Cdc42 has a much smaller threshold (inside the zone) and a higher (single) steady-state level inside the Rho zone, resulting in a broader Cdc42 zone that appears to overlap with the Rho zone.

Making and testing spatial predictions with the model

Given that spatial relationships are at the heart of pattern formation, we next sought to determine whether the model could be harnessed to predict the consequences of experimentally manipulating the spatial relationships of zones with each other. The most straightforward manner to accomplish this is to generate multiple wounds at different distances from each other such that zones are well separated, in close proximity, or overlapping. To investigate these manipulations in silico, we simulated Model 3 in two-dimensional space (see *Materials and Methods*) where two wounds are proximal to one another with additive initial stimuli.

Four sets of simulations were run (Supplemental Material, Section S7): those in which the distance between the wounds, L , was relatively large ($35 \mu\text{m}$), moderate ($26 \mu\text{m}$), small ($20 \mu\text{m}$), or very small ($1 \mu\text{m}$). Not surprisingly, at large distances, paired wounds behaved like single wounds, each encircled by one Cdc42 zone and one Rho zone (Figure 8A), a prediction that matches the behavior

observed in vivo (Figure 8A). Conversely, the model predicts that two very closely spaced wounds behave as a single wound, with the pair of holes becoming surrounded by a single set of zones, oval in shape (Figure 8B). Again, this prediction was matched by the in vivo result (Figure 8B).

However, between these two extremes, somewhat less intuitive results were predicted by the model. For paired wounds separated by a distance expected to result in overlapping of the Rho and the Cdc42 zones of adjacent wounds, the model predicted local annihilation of the Cdc42 zones by the Rho zones, such that two fused, ring-like Rho zones would be encircled by one approximately oval Cdc42 zone (Figure 8C). This predicted behavior was matched by the in vivo results (Figure 8C). This result is explained by recruitment of Abr to regions where Rho and Cdc42 are expected to overlap; Abr, once recruited, inactivates Cdc42 in this region.

Even less intuitive was the prediction for wounds positioned such that their Cdc42 zones were expected to be close (within ~5–10 μm) but not touching. The model predicted that in such cases, the two Cdc42 zones should reach across the space separating them and fuse (Figure 8D). Remarkably, this prediction too was confirmed by the in vivo results (Figure 8D). This result is explained by the stimuli from the two adjacent wounds adding together to breach the threshold concentration over a greater spatial extent between the wounds, yielding a fused zone wider than twice the width of single zones in controls.

DISCUSSION

Several specific findings emerge from the combined use of modeling and experiments in this study. The first is that the known interactions of Rho and Abr, if mediated by sufficiently nonlinear kinetics, are sufficient to explain the formation and maintenance of two spatially distinct activity levels, that is, the spatial bistability observed in this system. The second is that whereas the exclusion of active Cdc42 from the Rho zone can be explained by features of Abr, a nonlinear self-catalysis mechanism for Cdc42 activity control must be invoked to account for the observed bistability of the Cdc42. The third is that the models predict that the turnover rate of the GTPases is higher within the zones than in regions outside the zones, a finding that is initially counterintuitive but consistent with previous theoretical (Bement *et al.*, 2006) and empirical (Burkel *et al.*, 2012) observations.

Previous results obtained by analysis of the role of the dual GEF-GAP Abr provide the basis for positive feedback within the Rho zone: an initially shallow gradient of Rho activity would be autoamplified by the recruitment of Abr to the nascent Rho zone, where Abr would promote further Rho activation and thus further Abr recruitment (Vaughan *et al.*, 2011). How might nonlinear kinetics be incorporated into this scheme of feedback? Although the answer to this question awaits further analysis, potential explanations include increases in Abr Rho GEF activity due to plasma membrane targeting (e.g., Wang *et al.*, 2006), increased Rho GEF activity due to association of Abr with active Cdc42 via its GAP domain, or even increased Rho GEF activity due to association of active Rho via its GAP domain.

In the eventual Model 3, we chose a sigmoidal dependence of Cdc42 activation on Cdc42 activity level. To some extent, this choice (and detailed decisions about the nonlinear forms of the feedback terms) is arbitrary. It has been shown (Jilkin *et al.*, 2007, Appendix A; Kholodenko 2006) that various forms of positive feedback on GEFs are equivalent to negative feedback on GAPs, and that simultaneous Michaelian dependences on GTPase in both GEF and GAP rates also produce bistability (Kholodenko 2006). Linear terms do

not suffice, based on geometric arguments about the required nullcline shapes needed for multiple intersection points. We did not explore the exhaustive set of possible nonlinearities (but see Kholodenko, 2006, for a full classification using Michaelian terms alone) since the actual positive feedback mechanism responsible for maintenance of the Cdc42 zone remains to be identified experimentally, as does the exact nature of its nonlinear component. One reasonable possibility is that actin filament turnover is involved. This supposition is based on the recent demonstration that actin filament turnover is required for proper Cdc42 zone formation in wounded oocytes (Burkel *et al.*, 2012) and the demonstration of positive feedback between plasma membrane-associated actin filaments and Cdc42 activity in cultured cells expressing a bacterial Cdc42 GEF (Orchard *et al.*, 2012).

The basic model developed in this study not only faithfully recapitulates the basic features of zone amplification, segregation, and maintenance in the control situation, it also faithfully mimics several previously described manipulations, including expression of GEF- or GAP-dead Abr, inactivation of Rho via C3 exotransferase microinjection, and WT Abr overexpression. In each outcome (loss of bistability, broadening/thinning of zones), we can understand the results from the dynamical properties of the kinetic interactions between Rho, Abr, and Cdc42 (Figure 7).

Ideally, mathematical modeling generates predictions that are not obvious from empirical findings. The simulation of two adjacent wounds made one prediction that was semi-intuitive—that wounds placed close enough to result in the overlap of the Rho and Cdc42 zones would result in the local domination of the Rho zones, generating wounds with two merged Rho zones surrounded by a single Cdc42 zone. This result was confirmed empirically, although it remains possible that it reflects some other feature of the wound process. However, the two wound simulations made an additional prediction that is not at all intuitive and is harder to explain by other mechanisms: wounds made sufficiently close to bring the Cdc42 zones near each other without expected overlap were predicted to merge across the space separating each other. This prediction was confirmed by experiment, providing strong support both for the model and the utility of the approach. We therefore anticipate, as more players are added to the system by empirical studies, that their roles will be clarified by the application of the model.

In addition to the specific findings of this study, a more general result emerges, namely, the similarity of some of the basic findings concerning what is a cellular process to the multicellular events that characterize pattern formation in embryos. The general question—how is an initially crude signal (a local increase in calcium; Benink and Bement, 2005; Clark *et al.*, 2009) converted into more precisely ordered local signals such as the Rho GTPase zones?—is in essence the same question asked during embryonic pattern formation, in which initially broad, and broadly active, gradients of patterning information that span much of the system are progressively converted into narrow, and narrowly signaling, regions that may be just a few cells wide. This general similarity is consistent with the suggestion that the Rho GTPases be considered as core components of intracellular pattern formation systems, analogous to morphogens (Bement *et al.*, 2006; Goryachev, 2011), as well as recent work focused on determining how polarity is established after fertilization in *Caenorhabditis elegans* (Goehring *et al.*, 2011). Further, the finding of bistability in this system mirrors results obtained from analysis of BMP signaling in *Drosophila* (Wang and Ferguson, 2005; Umulis *et al.*, 2006), whereas the proposed model of zone segregation by Abr-dependent amplification of Rho and suppression of Cdc42 is reminiscent of the Notch–Delta signaling system in which

Notch-based signaling drives both its own amplification and the local suppression of antagonistic pathways (Artavanis-Tsakonas *et al.*, 1999).

There are, to be sure, several important differences between the intracellular pattern formation observed here relative to embryonic pattern formation, including speed (seconds to tens of seconds in this system, minutes to hours in embryos), less apparent dependence on transcriptional and translational mechanisms relative to embryos, and, of course, the fact that the changes controlled by the Rho GTPases are often reversible, whereas those of embryonic pattern formation are often irreversible. Nonetheless we think this analogy is a useful one, both because developmental pattern formation is a process familiar to many biologists and because of the specific examples provided by embryonic pattern formation, such as bistability. We think it likely that as more details emerge concerning examples of and mechanisms underlying Rho GTPase zones, this analogy will become increasingly useful.

MATERIALS AND METHODS

Experimental analysis

Oocyte collection and microinjection. Full-grown oocytes were obtained from adult *Xenopus laevis* frogs, manually defolliculated after collagenase treatment, and stored in a 1× Barth's solution as previously described (Benink and Bement, 2005). Oocytes were injected with mRNA encoding RFP-wGBD (to detect active Cdc42) or eGFP-rGBD (to detect active Rho) using a Harvard Apparatus p-100 microinjector and then allowed to express the mRNA overnight. GFP-rGBD and RFP-wGBD, respectively, were prepared and used as previously described (Benink and Bement, 2005) using mMessage machine kits (Ambion, Austin, TX).

Wounding, image acquisition, and image analysis. Movies highlighting GTPase zone movement were collected at six optical planes (1 fps) with a Zeiss Axiovert confocal microscope (Carl Zeiss, Jena, Germany) fitted with a nitrogen-pumped dye laser (Laser Science, Franklin, MA). Wounding was conducted as previously described (Benink and Bement, 2005). The 4D movies were rendered using Volocity (Improvision, PerkinElmer, Waltham, MA) and analyzed using ImageJ (National Institutes of Health, Bethesda, MD).

Modeling

Geometry. A typical wound radius is 10 μm, small by comparison to the oocyte diameter of ~1000 μm. Hence we approximate the wound region as flat. We also assume radial symmetry of all activity about the center of the wound.

Let r be radial distance, with $r = 0$ at the center of the wound and $r = w(t)$ at the wound edge, which evolves with time. Based on the relatively small size of the wound and the rapid diffusion of cytosolic GTPases relative to activation rates, the localized pattern should hardly deplete the cellular pool of GTPases, and we can approximate the levels of inactive RhoA, Cdc42, and Abr as fixed and spatially uniform (Supplemental Material, Section S1). Under these assumptions, we model the spatiotemporal concentration of active RhoA and Cdc42 anchored in the plasma membrane, differentiating between the active RhoA that is bound to Abr and the active RhoA that is free from Abr.

Interactions. In vitro (Chuang *et al.*, 1995) and in vivo (Vaughan *et al.*, 2011) experiments support interactions of RhoA, Cdc42, and Abr shown in Model 2 of Figure 3B. We denote the concentration G^j of the membrane forms and the cytosolic forms with superscripts

$j = a$ for active and $j = i$ for inactive, respectively. We consider $G^a(r, t)$ as the concentration of membrane-bound proteins in a measurement in a cylindrical shell about radius r that spans the cell diameter (Supplemental Material, Section S2). Before considering spatial effects, we start with a default balance equation for a well-mixed system, in which only activation (A_G) and inactivation (I_G) rates are considered (see Figure 3A). Then each active GTPase satisfies a differential equation of the form

$$\frac{dG^a}{dt} = f_G(G^i, G^a) = A_G G^i - I_G G^a \quad (1)$$

for $G = \text{Cdc42}$ or RhoA .

The rates A_G and I_G depend on GEF/(GAP and GDI) activity, as well as on feedback. We distinguish RhoA that is Abr bound from RhoA that is unbound. We keep track of only RhoA-bound Abr since Abr was found to have a tight spatiotemporal correlation with active RhoA, and, upon C3 exotransferase inhibition of RhoA, Abr recruitment was completely suppressed (Vaughan *et al.*, 2011), suggesting that binding to active Cdc42 and spontaneous localization to the plasma membrane are minimal. Abr is believed to have the ability to interact with RhoA and Cdc42 simultaneously (Chuang *et al.*, 1995), so the Abr-bound active RhoA is modeled to behave as a GEF/GAP for Cdc42. Further, Abr was shown to inhibit GTP dissociation (Chuang *et al.*, 1995), indicating that the inactivation rate of Abr-bound RhoA is less than that of unbound RhoA. Because the myriad of chemical species that regulate RhoA and Cdc42 (Pertz, 2010) are not explicitly accounted for, we coarse grain the reactions to express the activation/inactivation rates as functions of active Cdc42 and active Abr-bound/unbound RhoA. Our modeling approach is to assume simple, reasonable mathematical descriptions for each interaction in Figure 3B (Model 2) and then modify if needed. For example, since RhoA is activated by Abr, its rate of activation, $A_{\text{free rho}}$, should be an increasing function of RhoA-bound Abr. We begin by assuming that the forms of A and I are constants and successively test a sequence of assumptions such as linear, saturating (Michaelis-Menten), and sigmoidal (cooperative) kinetics. We selected the ultimate forms of A and I to exhibit the following properties.

Property 1: The proposed cross-talk scheme indicated in Figure 3B (Model 2) should be accounted for.

Property 2: The combination of terms should allow for both low and high RhoGTPase levels observed, respectively, far and close to the wound (spatial bistability). In the absence of a stimulus, cells have a low, stable, resting steady state in which no activity occurs.

Spatial distribution. We account for lateral diffusion of the membrane-bound proteins (with diffusion coefficient D). When actomyosin pulls the wound shut, we postulate that it advects membrane and proteins toward the wound. We write a balance equation for the concentration of each $G = \text{Cdc42}$ and Abr-bound/unbound RhoA for this reaction-diffusion-advection process:

$$\frac{\partial G^a}{\partial t} = \nabla \cdot (D \nabla G^a - v G^a) + f_G(\{G_k\})$$

where v is the velocity of membrane ingression toward the wound (due to myosin contraction, not explicitly modeled) and f_G is the rate of activation–inactivation given in Eq. 1, which can be a function of the other proteins to represent feedback. The wounded actin cortex is not capable of supporting GTPase activity, so we take no-flux or insulated boundary conditions at the wound edge

$([d/dr]G^a(w(t), t) = 0)$. The levels of the active proteins far away from the wound ($G^a(\infty, t)$) are assumed to be at low, basal steady-state values.

The rate at which the wound edge moves is equal to the advection velocity at the wound edge. That is, as the wound closes, the membrane fluid flows inwards with the boundary of the wound. The inward radial velocity of the membrane fluid obeys the continuity equation in two dimensions, which implies that the velocity is proportional to $1/r$. Mandato and Bement (2001) measured the instantaneous velocity of actin as a function of distance from the wound edge, and, even though 3D effects are present (inward ingression of the membrane and curvature effects), the radial velocity resembles a $1/r$ dependence. The magnitude of the velocity was chosen to yield a wound location that matches that of the data at the end of the simulation.

As noted, we initiate the model with RhoA and Cdc42 activity as found experimentally and shown at the point labeled $t = 0$ in Figure 2B (48 s after wounding in the experiment), when the initial wound edge is at $r = 8.82 \mu\text{m}$. Because the correlation between the intensity and concentration is unknown, we rescale the intensity but retain the spatial scales in Figure 2B (see the Supplemental Material, Section S11). The initial conditions are taken to be triangular peaks that resemble the intensity data at $t = 0$ and are shown in the first panel of Figure 5C. For the two wound simulations, a finite-volume package in Python, FiPy (Guyer *et al.*, 2009), is used to simulate Model 3 in 2D space. Gmsh is used to create the Swiss cheese-shaped mesh. Each wound has a similar initial condition to the radially symmetric simulations, except that where the initial condition of two wounds overlap, we consider them additive. No flux boundaries are taken at the wound edge and the outer boundary of the simulated box. As a simplifying approximation, advection and the moving boundary are ignored.

ACKNOWLEDGMENTS

We thank Nick Davenport and Alison Lewis (University of Wisconsin-Madison) and William Holmes, Nesy Tania, Ian Hewitt, and Laura Liao (University of British Columbia) for helpful discussions. This work was supported by a Natural Sciences and Engineering Research Council of Canada Discovery Grant (L.E.K.), National Institutes of Health Grant R01 GM086882 (Anders Carlsson, Principal Investigator), an International Graduate Training Center Fellowship from the Pacific Institute of Mathematical Sciences (C.S.), and National Institutes of Health Grant GM52932 (W.M.B.).

REFERENCES

Artavanis-Tsakonas S, Rand MD, Lake RJ (1999). Notch signaling: cell fate control and signal integration in development. *Science* 284, 770–776.

Bement WM, Benink HA, von Dassow G (2005). A microtubule-dependent zone of active RhoA during cleavage plane specification. *J Cell Biol* 170, 91–101.

Bement WM, Miller AL, von Dassow G (2006). Rho GTPase activity zones and transient contractile arrays. *Bioessays* 28, 983–993.

Benink HA, Bement WM (2005). Concentric zones of active RhoA and Cdc42 around single cell wounds. *J Cell Biol* 168, 429–439.

Bravo-Cordero JJ, Oser M, Chen X, Eddy R, Hodgson L, Condeelis J (2011). A novel spatiotemporal RhoC activation pathway locally regulates cofilin activity at invadopodia. *Curr Biol* 21, 635–644.

Burkel BM, Benink HA, Vaughan EM, von Dassow G, Bement WM (2012). A Rho GTPase signal treadmill backs a contractile array. *Dev Cell* 23, 384–396.

Chuang TH, Xu X, Kaartinen V, Heisterkamp N, Groffen J, Bokoch GM (1995). Abr and Bcr are multifunctional regulators of the Rho GTP-binding protein family. *Proc Natl Acad Sci USA* 92, 10282–10286.

Clark AG, Miller AL, Vaughan E, Yu HY, Penkert R, Bement WM (2009). Integration of single and multicellular wound responses. *Curr Biol* 19, 1389–1395.

Craciun G, Tang Y, Feinberg M (2006). Understanding bistability in complex enzyme-driven reaction networks. *Proc Natl Acad Sci USA* 103, 8697–8702.

Ferrell J Jr, Xiong W (2001). Bistability in cell signaling: how to make continuous processes discontinuous, and reversible processes irreversible. *Chaos* 11, 227–236.

Goehring NW, Trong PK, Bois JS, Chowdhury D, Nicola EM, Hyman AA, Grill SW (2011). Polarization of PAR proteins by advective triggering of a pattern-forming system. *Science* 334, 1137–1141.

Goryachev A (2011). A common mechanism for protein cluster formation. *Small GTPases* 2, 143–147.

Guyer JE, Wheeler D, Warren JA (2009). FiPy: partial differential equations with Python. *Comp Sci Eng* 11, 6–15.

Jaffe AB, Hall A (2005). Rho GTPases: biochemistry and biology. *Annu Rev Cell Dev Biol* 21, 247–269.

Jilkine A, Marée AFM, Edelstein-Keshet L (2007). Mathematical model for spatial segregation of the Rho-family GTPases based on inhibitory cross-talk. *Bull Math Biol* 69, 1943–1978.

Kholodenko B (2006). Cell-signaling dynamics in time and space. *Nat Rev Mol Cell Biol* 7, 165–176.

Ma C, Benink HA, Cheng D, Montplaisir V, Wang L, Xi Y, Zheng PP, Bement WM, Liu XJ (2006). Cdc42 activation couples spindle positioning to first polar body formation in oocyte maturation. *Curr Biol* 16, 214–220.

Machacek M, Hodgson L, Welch C, Elliott H, Pertz O, Nalbant P, Abell A, Johnson GL, Hahn KM, Danuser G (2009). Coordination of Rho GTPase activities during cell protrusion. *Nature* 461, 99–103.

Mandato CA, Bement WM (2001). Contraction and polymerization cooperate to assemble and close actomyosin rings around *Xenopus* oocyte wounds. *J Cell Biol* 154, 785–797.

Miller AL, Bement WM (2009). Regulation of cytokinesis by Rho GTPase flux. *Nat Cell Biol* 11, 71–77.

Orchard RC, Kittisopikul M, Altschuler SJ, Wu LF, Süel GM, Alto NM (2012). Identification of F-actin as the dynamic hub in a microbial-induced GTPase polarity circuit. *Cell* 148, 803–815.

Pertz O (2010). Spatio-temporal Rho GTPase signaling—where are we now? *J Cell Sci* 123, 1841–1850.

Postma M, Bosgraaf L, Looovers H, Van Haastert P (2004). Chemotaxis: signalling modules join hands at front and tail. *EMBO Rep* 5, 35–40.

Umulis DM, Serpe M, O'Connor MB, Othmer HG (2006). Robust, bistable patterning of the dorsal surface of the *Drosophila* embryo. *Proc Natl Acad Sci USA* 103, 11613–11618.

Vaughan EM, Miller AL, Yu HY, Bement WM (2011). Control of local Rho GTPase crosstalk by Abr. *Curr Biol* 21, 270–277.

Wang YC, Ferguson EL (2005). Spatial bistability of Dpp-receptor interactions during *Drosophila* dorsal-ventral patterning. *Nature* 434, 229–234.

Wang H, Yang C, Leskow FC, Sun J, Canagarajah B, Hurley JH, Kazanietz MG (2006). Phospholipase Cgamma/diacylglycerol-dependent activation of beta2-chimaerin restricts EGF-induced Rac signaling. *EMBO J* 25, 2062–2074.

Yoshida S, Bartolini S, Pellman D (2009). Mechanisms for concentrating Rho1 during cytokinesis. *Genes Dev* 23, 810–823.

Zhang X, Ma C, Miller AL, Katbi HA, Bement WM, Liu XJ (2008). Polar body emission requires a RhoA contractile ring and Cdc42-mediated membrane protrusion. *Dev Cell* 15, 386–400.